Journal of Sound and Vibration (1997) **203**(1), 41–62

A GLOBAL–LOCAL INTEGRATED STUDY OF ROLLER CHAIN MESHING DYNAMICS

S. P. Liu,† K. W. Wang, S. I. Hayek and M. W. Trethewey

The Pennsylvania State University, University Park, PA 16802, *U.S.A.*

AND

F. H. K. Chen

GM Research & Development Center, Warren, MI 48090, *U.S.A.*

(*Received* 30 *June* 1995, *and in final form* 28 *August* 1996)

It has been recognized that one of the most significant noise sources in roller chain drives is from impacts between the chain and the sprocket during their meshing process. In this paper an analysis is presented which integrates the local meshing phenomena with the global chain/sprocket system dynamic behavior. A coupled chain/sprocket system interacting with local impacts is modelled and the impulse function is derived. A study is carried out to quantify the intensity of subsequent impacts. It is found that the coupling effects between the sprockets, the chain spans, and the chain/sprocket meshing impulses increase with decreasing sprocket inertia and chain longitudinal stiffness. Experimental studies are also carried out to evaluate the meshing noise. It is found experimentally that the meshing sound pressure level is closely related to the chain speed and its vibrational characteristics, as predicted in the analytical study.

1. INTRODUCTION

While roller chain drives are recognized to be one of the most effective forms of power transmission in mechanical systems [1, 2], the noise and vibrations in such systems can be a problem [3], especially since higher speed, lighter weight and higher quality are required in today's products.

Major noise sources in roller chain drive systems have been identified experimentally by Uehara and Nakajima [4]. It was concluded that the most significant source is from the impact between the chain link and the sprocket tooth during the meshing process. It was found that the impact noise is closely related to the overall dynamic behavior of the chain and various system parameters, such as chain tension, speed, and pitch. An experimental study by Stone, Trethewey and Wang [5] also showed that the noise level and the impact intensity during meshing are closely correlated. Several researchers [6–9] have studied the impulses caused by the meshing impact when a single roller engages the driving sprocket. These analyses assumed that the chain/sprocket relative velocity at meshing is constant and the impulse is computed with the chain straight and stationary. The impact inertia is, therefore, evaluated under a quasi-static condition of the chain.

Through integrating the local meshing characteristics with the response of a vibrating axially moving chain, a recent study by Wang *et al*. [10] found that significant errors will be induced in computing the impact intensity using the classical quasi-static approach, in which the vibration of the travelling chain is neglected. While this investigation has

† Currently at Mechanical Dynamics, Inc.

0022–460X/97/210041 + 22 $25.00/0/sv960792

provided new insights, the analysis is limited to a single chain transverse vibration model. The direction of the relative velocity between the meshing sprocket tooth and chain link is assumed to be perpendicular to the chain span. Also, the chain longitudinal motion is not considered. Since the chain longitudinal vibration is important to the overall system dynamic behavior under certain conditions [7, 11–13], the study by Wang *et al*. [10] needs to be expanded: that is, both the longitudinal and transverse chain motions should be included in quantifying the meshing impulses. Because these two motions are coupled through the sprocket dynamics [14], an integrated chain/sprocket system model is required to carry out the investigation.

In this paper an integrated study of a coupled chain/sprocket system under repeating impacts from the meshing process is presented. Both analytical and experimental efforts have been performed. This investigation provides a basic understanding and additional insights to the roller chain meshing dynamics, which is an essential step towards the design of quiet chain drives.

2. SYSTEM MODEL

2.1. FORMULATION

A schematic of the model is illustrated in Figure 1 (a list of nomenclature is given in Appendix D). The chain drive is modelled as two axially moving strings with their ends fixed to two rigid sprockets. The fixed–fixed boundaries are defined at both seated rollers, $x = 0$ and $x = L$. Assumptions defining this problem are as follows.

(1) The displacement of the chain spans and the motion of the sprockets are measured from an initial constant tension, constant speed, constant driving and driven loads, axially moving chain configuration, and the corresponding constant speed condition of the sprockets.

(2) The impulsive loads are applied at the meshing rollers of both chain spans with an angle between 0 and 90 degrees from the span (Figure 1).

(3) Constant torque inputs are applied to the driving and driven shafts.

(4) Clearance and slipping between the chain and the sprocket are neglected.

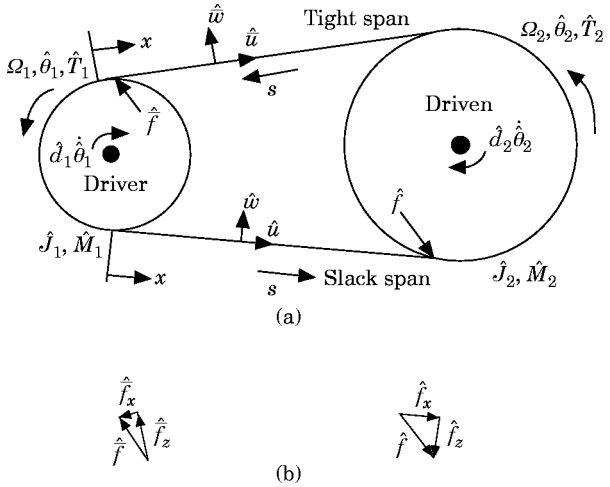

Figure 1. (a) A schematic of the system model. (b) $\hat{\bar{f}}$ and $\hat{f}$ are the impulses with the components shown.

(5) The initial tension difference between the tight and the slack side of the chain drive is balanced by the torsional damping force of the sprockets and the constant driving/driven torques under the initial constant speed condition.

(6) Out-of-plane motion of the chain is not considered.

(7) Both the longitudinal and transverse motions of the chain are included in the model.

(8) Dependent variable variations are significant only in the axial, x-direction.

The equations of motion are derived via Hamilton's principle. The outline of the derivation is shown in Appendix A. With the non-dimensional variables listed in Appendix C, the linearized system equations of motion for $0 < \xi < 1$, and $\tau \geqslant 0$ with rigid supports at the sprockets are

$$\ddot{\bar{u}} + \bar{d}_x\dot{\bar{u}} - 2v\dot{\bar{u}}' - \Phi\bar{u}'' = -\bar{f}_x, \qquad \ddot{u} + d_x\dot{u} + 2v\dot{u}' - \Phi u'' = f_x, \tag{1, 2}$$

$$\ddot{\bar{w}} + \bar{d}_z\dot{\bar{w}} - 2v\dot{\bar{w}}' - \Psi\bar{w}'' = \bar{f}_z, \qquad \ddot{w} + d_z\dot{w} + 2v\dot{w}' - \Psi w'' = -f_z, \tag{3, 4}$$

Here, $\bar{f}_x$ and f_x, defined in Appendix B, are the axial components of the impulsive forces for the tight span and slack span, respectively. Also, $\bar{f}_z$ and f_z, given in Appendix B, represent the transverse components of the impulsive forces for the tight and slack spans, respectively. As shown in Figure 1, the total impulsive forces applied to the chain spans are

$$\bar{f} = \sqrt{\bar{f}_x^2 + \bar{f}_z^2}, \qquad f = \sqrt{f_x^2 + f_z^2}. \tag{5}$$

The associated boundary conditions are

$$\bar{u}_0 + u_0 = 0, \qquad -\alpha(\bar{u}_0' - u_0') - \frac{J_1}{2\rho_1^2}(\ddot{u}_0 - \ddot{\bar{u}}_0) - \frac{d_1}{2\rho_1^2}(\dot{u}_0 - \dot{\bar{u}}_0) = 0, \tag{6, 7}$$

$$\bar{u}_1 + u_1 = 0, \qquad -\alpha(\bar{u}_1' - u_1') - \frac{J_2}{2\rho_2^2}(\ddot{u}_1 - \ddot{\bar{u}}_1) - \frac{d_2}{2\rho_2^2}(\dot{u}_1 - \dot{\bar{u}}_1) = 0, \tag{8, 9}$$

$$w_0 = \bar{w}_0 = 0, \qquad w_1 = \bar{w}_1 = 0, \tag{10, 11}$$

where the dot and prime denote derivatives with respect to the non-dimensional time τ and space ξ, respectively, and $u_0 = u(0, \tau)$, $w_0 = w(0, \tau)$, $u_1 = u(1, \tau)$, $w_1 = (1, \tau)$, $\bar{u}_0 = \bar{u}(0, \tau)$, $\bar{w}_0 = \bar{w}(0, \tau)$, $\bar{u}_1 = \bar{u}(1, \tau)$ and $\bar{w}_1 = \bar{w}(1, \tau)$.

2.2. DISCRETIZATION

Because equations (1)–(4) and (6)–(11) cannot be solved exactly, Galerkin's method is employed. For this system, the trial functions selected for u and $\bar{u}$ are the *eigenfunctions* of the stationary undamped system ($v = 0$) described by equations (1), (2) and (6)–(9). These functions are

$$\bar{h}_n(\xi) = \sin\beta_n\xi = h_n(\xi), \qquad n = 1, 3, 5, \ldots,$$

$$\bar{h}_n(\xi) = -\frac{J_1\beta_n}{2\rho_1^2}\sin\beta_n\xi + \cos\beta_n\xi = -h_n(\xi), \qquad n = 0, 2, 4, \ldots, \tag{12}$$

where β_n are the *eigenvalues* obtained from the *characteristic equations*,

$$\sin\beta_n = 0, \qquad \beta_n = n\pi, \qquad n = 0, 1, 2, 3, \ldots \tag{13a}$$

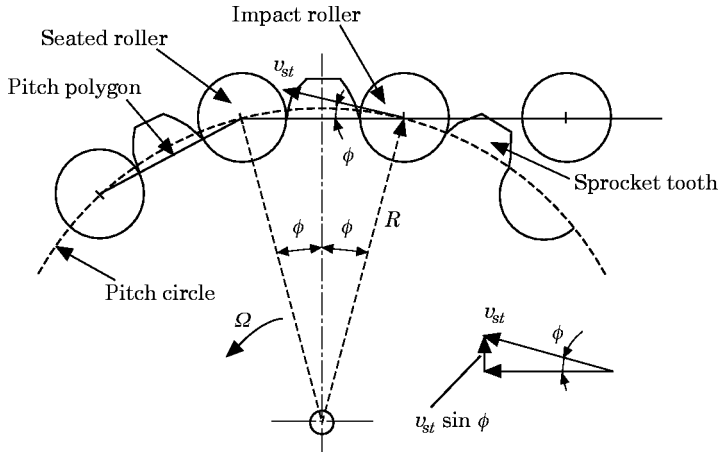

Figure 2. The roller chain/sprocket configuration at meshing.

and

$$\tan \beta_n = \frac{2\beta_n(J_2\rho_1^2 + J_1\rho_2^2)}{(J_1J_2\beta_n^2 - 4\rho_1^2\rho_2^2)}, \qquad n = 1, 2, 3, \ldots . \tag{13b}$$

w and $\bar{w}$ are expanded by the comparison functions $\bar{b}_n(\xi) = b_n(\xi) = \sin(n\pi\xi)$ $(n = 1, 2, 3, \ldots)$ which satisfy the fixed–fixed boundary conditions (10) and (11). Using Galerkin's method, the discretized weak form is obtained from

$$\langle e_{d1}, \bar{h}_m(\xi)\rangle + \sum_{j=1}^{4} (e_{bj} \cdot \bar{h}_{bm}) = 0, \qquad \langle e_{d2}, h_m(\xi)\rangle + \sum_{j=1}^{4} (e_{bj} \cdot h_{bm}) = 0,$$

$$\langle e_{d3}, \bar{b}_m(\xi)\rangle = 0, \qquad \langle e_{d4}, b_m(\xi)\rangle = 0,$$

where $m = 1, 2, , \ldots, M$ are the number of Galerkin's expression terms, and $\langle , \rangle$ represents an unweighted inner product in the domain $0 < \xi < 1$. e_{d1}, e_{d2}, e_{d3} and e_{d4} are the residuals from equations (1)–(4), respectively. $\bar{h}_{bm}$ and h_{bm} are the values of $\bar{h}_m(\xi)$ and $h_m(\xi)$ at boundaries $\xi = 0$ and $\xi = 1$ where the corresponding boundary conditions (6)–(9), e_{bj}, are evaluated.

2.3. DERIVATION OF THE IMPULSE FUNCTION

A schematic of the roller and sprocket configuration is shown in Figure 2. The impulse caused by the meshing process is a function of the relative velocity between the sprocket and the chain roller at the instant of impact. The momentum balance method, which has been used in solving various flexible body impact problems [15, 16], is employed to derive the impulse amplitude under the following assumptions.

(1) The inertia of the sprocket is much greater than that of the chain roller. The sprocket angular velocity is thus not affected by the impact.

(2) The impact load is assumed to be uniformly applied on the chain between $\xi = \xi_1$ and $\xi = \xi_2$ on the tight span, and chain between $\xi = \xi_1'$ and $\xi = \xi_2'$ on the slack span. The center of the impact roller is at $\xi_0 = (\xi_2 + \xi_1)/2$ (corresponding to one pitch length x_0) for the tight span, and $\xi_0' = (\xi_2' + \xi_1')/2$ for the slack side.

(3) The impact is inelastic, and the velocity of the impact roller coincides with that of the sprocket V_{st} immediately after impact. The sprocket does not constrain the chain motion before or after an impact. Here, V_{st} denotes the tangential speed of the sprocket tooth at the sprocket pitch circle.

Let $w(\xi, \tau) = \Sigma_{n=1}^{\infty} b_n(\xi) q_n(\tau)$. The discretized weak form of equation (4) yields

$$M_w \ddot{q}(\tau) + (G_w + D_w)\dot{q}(\tau) + K_w q(\tau) = Y_w \sum_{k=1}^{N} I_{zk}\, \delta(\tau - \tau_k), \tag{14}$$

where $q(\tau) = [q_1, q_2, \ldots, q_n]^{\mathrm{T}}$ is the generalized displacement vector, and $\dot{q} = \mathrm{d}q/\mathrm{d}\tau$. M_w, G_w, D_w and K_w are the inertia, gyroscopic, damping and stiffness matrices, respectively, and Y_w is a space vector (see Appendix B). I_{zk} are the transverse components of the impulses on the slack side of the chain span. Integrating equation (14) over the kth impact duration ($\tau = \tau_k^-$ to τ_k^+), we have

$$\int_{\tau_k^-}^{\tau_k^+} (M_w \ddot{q}(\tau) + (G_w + D_w)\dot{q}(\tau) + K_w q(\tau))\, d\tau = Y_w \int_{\tau_k^-}^{\tau_k^+} \sum_{k=1}^{N} I_{zk}\, \delta(\tau - \tau_k)\, \mathrm{d}\tau. \tag{15}$$

Since the configuration of the chain is assumed to be invariant during the small duration of the impact, equation (15) becomes

$$M_w(\dot{q}(\tau_k^+) - \dot{q}(\tau_k^-)) = Y_w I_{zk}. \tag{16}$$

For the nth row of equation (16), one has

$$\dot{q}_n(\tau_k^+) = M_w^{-1} Y_w I_{zk} + \dot{q}_n(\tau_k^-). \tag{17}$$

From the previous assumptions, the transverse velocity of the meshing roller over the range (ξ_1', ξ_2') is approximated by the velocity at ξ_0', and is assumed to be of the value V_{sw} (the transverse component of the sprocket tooth velocity) immediately after impact. Thus, one has

$$\frac{\mathrm{d}w(\xi_0', \tau_k^+)}{\mathrm{d}\tau} = \dot{w}(\xi_0', \tau_k^+) + v w'(\xi_0', \tau_k^+) = -V_{sw}$$

and

$$\sum_{n=1}^{M} \dot{q}_n(\tau_k^+) b_n(\xi_0') = -V_{sw} - v w'(\xi_0', \tau_k^+). \tag{18}$$

Substituting equation (17) into equation (18), one can derive

$$M_w^{-1} Y_w b_n(\xi_0') I_{zk} = -V_{sw} - \sum_{n=1}^{M} b_n(\xi_0') \dot{q}_n(\tau_k^-) - v w'(\xi_0', \tau_k^+). \tag{19}$$

Since the displacement field does not change during impact, i.e.,

$$w'(\xi_0', \tau_k^+) = w'(\xi_0', \tau_k^-),$$

equation (19) becomes

$$M_w^{-1} Y_w b_n(\xi_0') I_{zk} = -V_{sw} - \frac{\mathrm{d}w(\xi_0', \tau_k^-)}{\mathrm{d}\tau}. \tag{20}$$

Therefore, the kth transverse component of the impulse on the slack span is

$$I_{zk} = \frac{-V_{sw} - \mathrm{d}w(\xi_0', \tau_k^-)/\mathrm{d}\tau}{M_w^{-1} Y_w b_n(\xi_0')}. \tag{21}$$

Carrying out similar derivations as above, one can derive the other impulse components as follows:

$$\bar{I}_{zk} = \frac{V_{s\bar{w}} - \mathrm{d}\bar{w}(\xi_0, \tau_k^-)/\mathrm{d}\tau}{M_{\bar{w}}^{-1} Y_{\bar{w}} \bar{b}_n(\xi_0)}, \qquad \bar{I}_{xk} = \frac{-(V_{s\bar{u}} - (v - \mathrm{d}\bar{u}(\xi_0, \tau_k^-)/\mathrm{d}\tau))}{M_{\bar{u}}^{-1} Y_{\bar{u}} \bar{h}_n(\xi_0)}, \tag{22, 23}$$

$$I_{xk} = \frac{V_{su} - (v + \mathrm{d}u(\xi_0', \tau_k^-)/\mathrm{d}\tau)}{M_{\bar{u}}^{-1} Y_u h_n(\xi_0')}, \tag{24}$$

The resultant impulses of the slack and tight spans are, respectively,

$$I_k = \sqrt{I_{xk}^2 + I_{zk}^2}, \qquad \bar{I}_k = \sqrt{\bar{I}_{xk}^2 + \bar{I}_{zk}^2}. \tag{25, 26}$$

Here, $\bar{I}_{xk}$ and I_{xk} are the axial components of the impulses on the tight and slack spans respectively, and $\bar{I}_{zk}$ represents the transverse impulse on the tight span. $M_{\bar{u}}$, M_u and $M_{\bar{w}}$ are mass matrices, while $Y_{\bar{u}}$, Y_u and $Y_{\bar{w}}$ are space vectors given in Appendix B. $V_{s\bar{u}}$ and V_{su} denote the axial components of sprocket tooth velocities at impact points on the tight and slack spans, respectively; meanwhile, $V_{s\bar{w}}$ is the transverse component on the tight span (see Appendices C and D). Note that the sprocket angular velocity is affected by the chain longitudinal response through the boundary conditions. Thus, the sprocket velocity components are not constant for different meshing impacts.

2.4. IMPLICATION OF THE MODEL

Examining equations (1)–(4), one can see that the four field variables, (i.e., w, $\bar{w}$, $\bar{u}$ and u), are not explicitly coupled. In fact, they are implicitly coupled through the impulse functions (21)–(24). The chain longitudinal motion affects the sprocket motion which determines the sprocket tooth velocity. The sprocket tooth velocity affects the impact intensities in both the longitudinal and transverse directions. The impact intensity affects the chain span motion. Consequently, the impact dynamics, the chain transverse and longitudinal motions, and the sprocket motion are closely coupled.

3. A SIMPLIFIED MODEL

In equations (21)–(24), the impact intensities are functions of sprocket rotational speeds and chain span motions. The chain span motions are coupled at the chain span boundaries through sprockets as shown in equations (6)–(9). The degree of this coupling is determined by the non-dimensional system parameters, sprocket inertias (J_1 and J_2) and longitudinal chain stiffness (α). It can be shown that when J_1 and $J_2 \to \infty$, the longitudinal chain span response at the boundaries will be reduced to zero ($\bar{u}_0 = u_0 = 0$ and $\bar{u}_1 = u_1 = 0$). The system can thus be treated as two separated axially moving chain spans with fixed–fixed boundaries. This indicates that there is no chain span response coupled through the sprockets at the boundaries. The sprockets are not oscillating and maintain a constant operating speed. If the longitudinal chain stiffness (α) is also large ($\alpha \to \infty$) in this case, the longitudinal chain response can be assumed to be quasi-static. Under this condition,

$\bar{I}_{xk}$ and I_{xk} in equations (23) and (24) can be neglected because the relative impact velocities are negligible. Therefore, the resultant impulses are assumed to be perpendicular to the chain spans (i.e., $I_k = I_{zk}$ and $\bar{I}_k = \bar{I}_{zk}$), and the model is simplified to the one derived in Wang *et al*. [10]. In other words, the system in equations (1)–(4) and (6)–(11) can be reduced to two decoupled transverse chain span equations (3) and (4) with the boundary conditions (10) and (11).

On the other hand, when J_1, J_2 and α are small, coupling effects of the chain spans and sprockets on the engagement impulses could be significant. The following sections further investigate these system parameters effects on the chain/sprocket impact dynamics in a two-sprocket chain drive system.

4. ANALYSIS AND DISCUSSION

For the purpose of discussion, all parameters used in the following discussion are non-dimensionalized with definitions given in Appendices C and D. The parameters used in analyzing the system dynamics are listed in Table 1 unless stated differently. We define an average impulse

$$\hat{I}_{avg} = \frac{\sum_{k=N_0}^{N} \hat{I}_k}{N - N_0 + 1}$$

to be the mean intensity of the subsequent impacts, where $\hat{I}_k$ can be any one of the subsequent impact intensities given in equations (21)–(26). In the following studies, N_0 is selected to be sufficiently large such that $\hat{I}_k$ is at steady state for $k > N_0$.

4.1. EFFECTS OF CHAIN RESONANT AND MESHING FREQUENCIES ON IMPACT INTENSITY

4.1.1. *Simplified model*

Given an initial transverse impact with impulse $\bar{I}_{z1}$, the chain's tranverse velocity time response $\mathrm{d}\bar{w}(\xi_0, \tau)/\mathrm{d}\tau$ is plotted in Figure 3. It is shown that at times τ_a, τ_b, τ_c and τ_d, the velocity is negative. Therefore, if the chain/sprocket meshing period τ_I coincides with these values, the next impulse $\bar{I}_{z2}$ will be relatively large since the difference between $V_{s\bar{w}}$ and $\mathrm{d}\bar{w}(\xi_0, \tau_2^-)/\mathrm{d}\tau$ is high (see equation (22)). Based on the same reasoning, $\bar{I}_{z2}$ will be relatively

TABLE 1

System parameters

$\bar{R} = 415$ N	$R = 268$ N	$EA = 261\,300$ N
$x_0 = 0{\cdot}0095$ m	$L = 0{\cdot}225$ m	$m = 0{\cdot}7516$ kg/m
$\hat{J}_1 = 0{\cdot}034$ kg m^2	$\hat{J}_2 = 0{\cdot}2397$ kg m^2	
$r_1 = 0{\cdot}029$ m	$r_2 = 0{\cdot}058$ m	

Sprocket center to center distance = 0·1905 m
Numbers of driving/driven sprocket teeth = 19 and 38

Non-dimensional parameters

$\xi_0 = 0{\cdot}05$	$\xi_0' = 0{\cdot}95$	$\xi_1 = 0{\cdot}0375$
$\xi_1' = 0{\cdot}9625$	$\xi_2 = 0{\cdot}0625$	$\xi_2' = 0{\cdot}9375$
$d_x = d_{\bar{x}} = 0$	$d_z = d_{\bar{z}} = 0{\cdot}02\pi$	$d_1 = d_2 = 0$

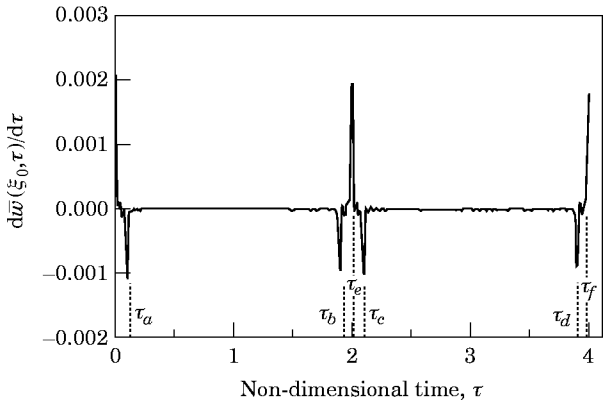

Figure 3. The time history of the chain transverse velocity at $\xi = \xi_0$ after the initial impact.

small when the meshing period is equal to τ_e or τ_f. Note here that τ_e is the fundamental natural period of the chain transverse vibration, τ_1, and $\tau_f = 2\tau_e = 2\tau_1$.

Examining the chain transverse $d\bar{w}(\xi_0, \tau)/d\tau$ under subsequent impacts (Figure 4), we see that when the meshing frequency is equal to the chain span fundamental natural frequency, $f_I = 1/\tau_e = 1/\tau_1$, the impacts always take place when $d\bar{w}(\xi_0, \tau_k^-)/d\tau$ is positive and close to the $V_{s\bar{w}}$ value. For $f_I = 1/\tau_b$, impacts always occur at points at which $d\bar{w}(\xi_0, \tau_k^-)/d\tau$ is negative. To illustrate further the magnitude of subsequent impacts of a travelling chain at different meshing frequencies, three cases are presented in Figure 5. The

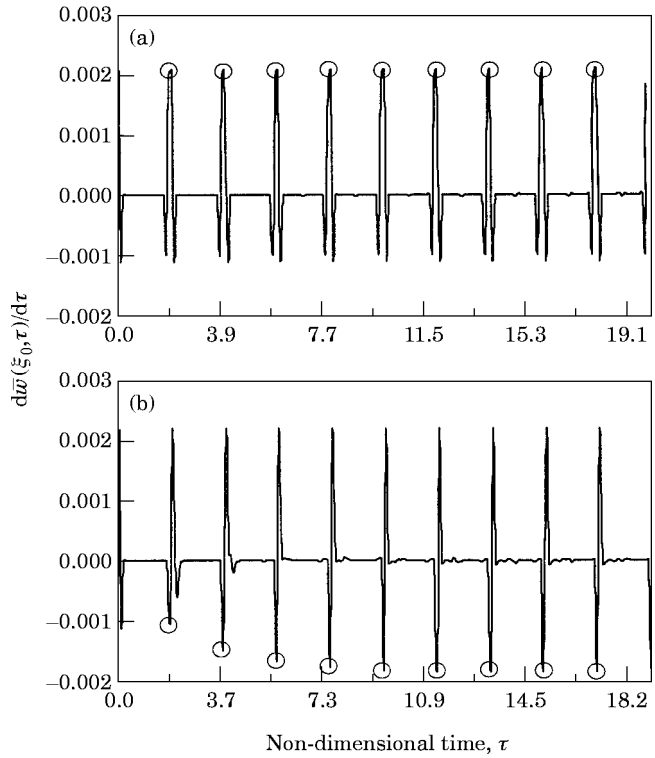

Figure 4. The time history of the chain transverse velocity at $\xi = \xi_0$ under subsequent impacts. ○, Time at which impact occurs with a chain velocity $d\bar{w}(\xi_0, \tau_k^-)/d\tau$. (a) $f_I = 1/\tau_e$; (b) $f_I = 1/\tau_b$.

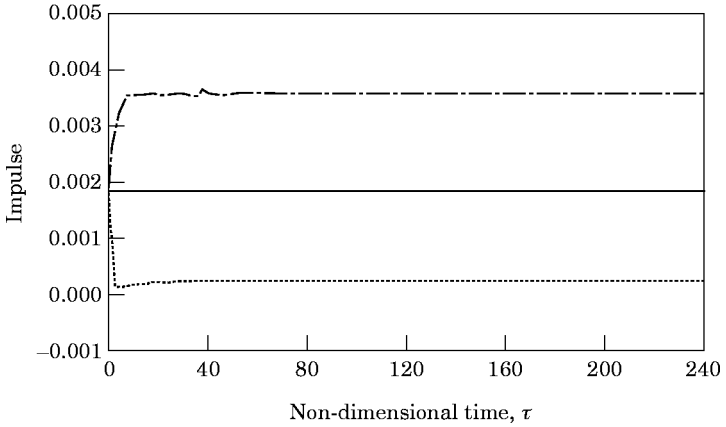

Figure 5. Subsequent impulses for different meshing frequencies. –·–·-, $f_I = 1/\tau_b$; ——, $\hat{I}_0$; ····, $f_I = 1/\tau_e$.

impulse $\hat{I}_0$ is derived from a quasi-static non-vibrating chain model, similar to results in the previous study by Chew [6]. Since $\hat{I}_0$ is not affected by the chain response, it is constant with respect to time. The other $\bar{I}_{zk}$ values in Figure 5 are computed based on equation (22). Here, it is shown that the impulse function eventually reaches a steady state value. For $f_I = 1/\tau_e = 1/\tau_1$, $\bar{I}_{zk}$ is much smaller when compared to other cases. $\bar{I}_{zk}$ reaches its maximum value when $f_I = 1/\tau_b$. These observations indicate that the quasi-static approach could create significant errors in predicting the impact intensity, and that the results derived from the last paragraph can be extended to quantify the meshing impulses of the chain under subsequent impacts.

Based on the numerical results shown in Figures 3–5 and the above discussions, one can conclude the following: (1) For $\tau_1 = m\tau_e/n = m\tau_1/n$ (m and n are positive integers), the impact roller velocity $\mathrm{d}\bar{w}(\xi_0, \tau_k^-)/\mathrm{d}\tau$ will eventually reach a steady state positive value which is close to $V_{s\bar{w}}$. The velocity difference, $V_{s\bar{w}} - \mathrm{d}\bar{w}(\xi_0, \tau_k^-)/\mathrm{d}\tau$, is thus relatively small, and the impulse caused by the chain/sprocket meshing process will therefore be relatively small under these conditions.

(2) For $\tau_1 = \tau_a/n$, τ_b/n, τ_c/n or τ_d/n (n is a positive integer), the steady state $\mathrm{d}\bar{w}(\xi_0, \tau_k^-)/\mathrm{d}\tau$ will be negative with relatively large absolute values. The impulse caused by the chain/sprocket meshing process will therefore be relatively large under these conditions.

4.1.2. *Complete model*

The relationship between the chain resonant frequency, the meshing frequency and the impact intensity in equations (21)–(24) is more complicated than that in the simplified model. When the longitudinal impacts are present in the system, the sprocket rotational speeds are not constant. The resultant impulses in equations (25) and (26) will depend on the amplitude and phase of the chain span velocity as well as that of the sprocket tangential speed at the instant of impact. Generally speaking, the chain resonant frequency and meshing frequency effects on the transverse impulses discussed in the simplified model are still applicable if the sprocket speed variation is small. That is, I_{zk} or $\bar{I}_{zk}$ will be near its local minimum when the meshing periods correspond to $\tau_I = m\tau_e/n = m\tau_1/n$ (m and n are positive integers), and will be near its local maximum when the meshing period corresponds to $\tau_1 = \tau_a/n$, τ_b/n, τ_c/n or τ_d/n (n is a positive integer), as shown in Figure 3 (here, τ_a, τ_b, τ_c, τ_d and τ_e are different for the tight and slack spans). However, the resultant impulse is also dependent on the magnitude of the longitudinal impulse. In general, the transverse fundamental natural period of the chain span can be different from the longitudinal one.

Therefore, the local maximum or minimum of the transverse impulse will not coincide with that of the longitudinal impulse.

For the purpose of discussion, let the longitudinal fundamental natural frequency of the chain span equal to that of the transverse natural frequency. Given an initial longitudinal impact with impulse $\bar{I}_{x1}$ ($I_{xk} = I_{zk} = \bar{I}_{zk} = 0$), the time history of $\mathrm{d}\bar{u}(\xi_0, \tau)/\mathrm{d}\tau$ (rate of longitudinal deformation) is plotted in Figure 6(a). It is shown that at times τ_a, τ_b, τ_c, τ_d and τ_e, $\mathrm{d}\bar{u}(\xi_0, \tau)/\mathrm{d}\tau$ is not zero. These variations will change the relative impact velocities of the subsequent longitudinal impacts. In Figure 6(b), it is shown that the sprocket's tangential speed is oscillating after an initial longitudinal impact. In equation (23), the relative impact velocity is a function of the sprocket tangential speed component in the chain axial direction. Therefore, if the chain/sprocket meshing period τ_1 coincides with these peak values (i.e., $\tau_I = \tau_a$, τ_b, τ_c, τ_d and τ_e) and if the phase of the sprocket tangential speed variation is opposite to that of the chain longitudinal deformation rate at the impact location, the next impulse $\bar{I}_{x2}$ will be relatively large since the difference between $V_{s\bar{u}}$ and $(v - \mathrm{d}\bar{u}(\xi_0, \tau_2^-)/\mathrm{d}\tau)$ is large. With the same reasoning, $\bar{I}_{x2}$ will be relatively small when the meshing period is equal to the values in which the sprocket tangential speed variation and the chain longitudinal deformation rate are zero.

The coupling phenomena between the tight and the slack chain spans are shown in Figure 6(c). The travelling wave created by the initial longitudinal impact on one side of the chain span is partially transmitted to the other side through the sprocket. The

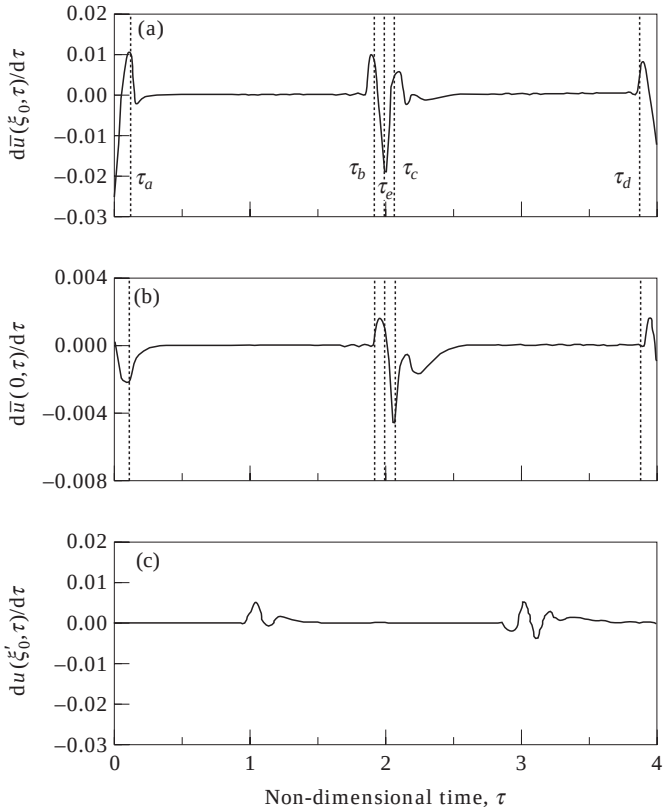

Figure 6. (a) The time history of the chain tight span longitudinal deformation rate at $\xi = \xi_0$ after the initial impact with $J_1 = J_2 = 0{\cdot}01$ and $\alpha = 1$. (b) The sprocket tangential speed variation. (c) The time history of the chain slack span longitudinal deformation rate at $\xi = \xi_0'$ after the initial impact with $J_1 = J_2 = 0{\cdot}01$ and $\alpha = 1$.

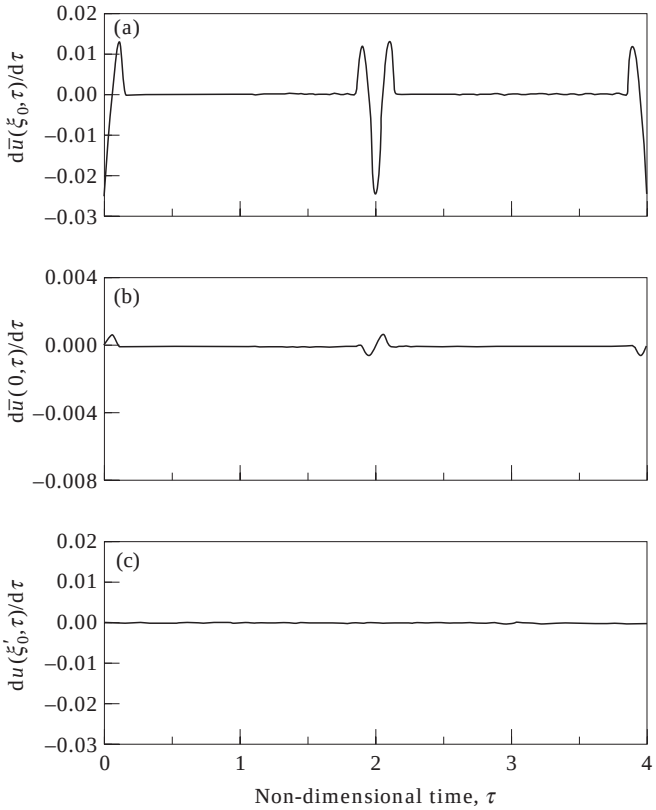

Figure 7. (a) The time history of the chain tight span longitudinal deformation rate at $\xi = \xi_0$ after the initial impact with $J = J_2 = 1$ and $\alpha = 1$. (b) The sprocket tangential speed variation. (c) The time history of the chain slack span longitudinal deformation rate at $\xi = \xi_0'$ after the initial impact with $J_1 = J_2 = 1$ and $\alpha = 1$.

transmitted travelling wave could affect the impact dynamics on the other side of the chain span. The amplitude of this transmitted wave will depend on the sprocket inertias (J_1 and J_2) and the longitudinal chain stiffness (α).

The coupling phenomena between the chain spans and the sprocket with a larger sprocket inertia are further shown in Figures 7(a)–(c). It is shown that the amplitude of the sprocket tangential speed oscillation decreases as the sprocket inertia increases. The travelling wave is reflected mostly from the chain-span's boundary, with very little being transmitted to the slack side of the chain span. This illustrates that the degree of the coupling between the chain spans and the sprocket motions is affected by the sprocket inertia.

Since both the longitudinal and transverse impacts are considered, meshing dynamics of the complete model become very complicated. In general, one can predict that: (1) the resultant impact intensity will have its local maximum when both the transverse and longitudinal impulse components are at their local maxima; and (2) the resultant impact intensity will have its local minimum when both the transverse and longitudinal impulse components are at their local minima.

4.2. DISCUSSION AND COMPARISON BETWEEN MODELS

To illustrate further the effect of the chain span and sprocket motions on the impact intensity, time histories of the subsequent longitudinal and transverse impacts of the tight

span ($\bar{I}_{xk}$ and $\bar{I}_{zk}$) are shown in Figure 8. The meshing frequency is equal to the fundamental natural frequencies of both the longitudinal and the transverse chain motions ($f_I = 1/\tau_e$). In this case, the transverse impulse will have its local minimum, but the longitudinal impulse will be relatively large. It is shown that the amplitudes of the longitudinal impacts are oscillating. These oscillations indicate that the resultant relative impact velocities fluctuate and, therefore, directions of the resultant impulses also fluctuate. Note that the simplified model cannot predict these changes in the impulse directions. It is also shown that the absolute values of the longitudinal impulses are larger than those of the transverse impulses in this specific case. In Figure 9 the time history of the resultant impulses computed from Figure 8 is compared with the impulses (transverse directions only) of the simplified model. It is shown that the resultant impulses oscillate with amplitudes larger than those of the impulses computed from the simplified model. This is because, while the transverse impulse is near to a local minimum value, the resultant impulse can produce a large value due to the large longitudinal impulse.

To gain further insight, an example is illustrated in Figure 10. Here, the averaged resultant impulses of the tight span are plotted for various α. The simplified model does not include the sprockets' inertias, and considers the transverse impulses of the chain span only. Therefore, its averaged impulses are constant with respect to α at a constant sprocket rotational speed. It is shown that as α decreases, the averaged resultant impulses tend to increase and diverge from the averaged impulses of the simplified model. This indicates that the sprocket dynamics and chain longitudinal motions become important in predicting impulses when α is small. On the other hand, the averaged resultant impulses fluctuate and converge to the averaged impulses of the simplified model as α increases. From equations (21)–(24), it is shown that the impulse functions depend on the responses of both the

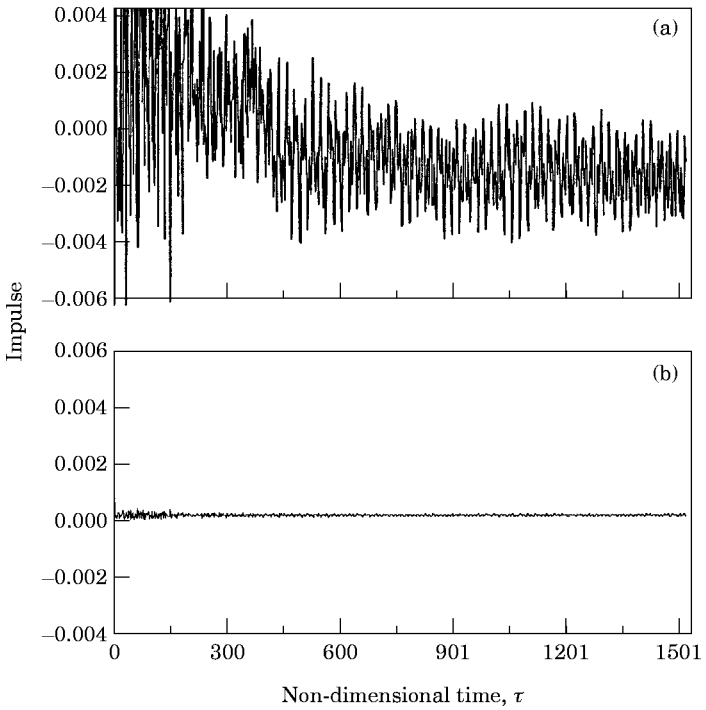

Figure 8. The time history of the subsequent impacts with $J_1 = J_2 = 0{\cdot}01$ and $\alpha = 1$ at meshing frequency $f_I = 1/\tau_e$. (a) Longitudinal impulses, $\bar{I}_{xk}$; (b) transverse impulses, $\bar{I}_{zk}$.

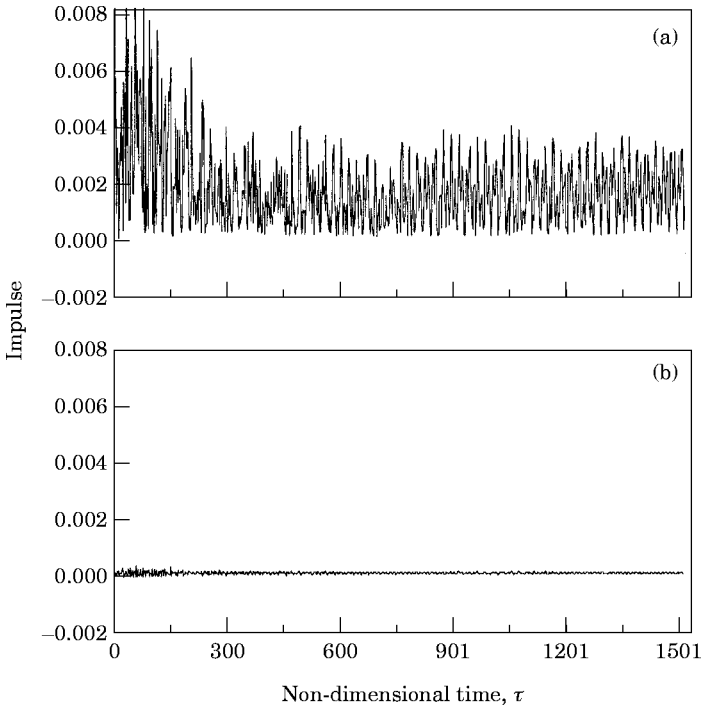

Figure 9. The time history of the subsequent impacts with $J_1 = J_2 = 0{\cdot}01$ and $\alpha = 1$ at meshing frequency $f_l = 1/\tau_e$. (a) Resultant impulses $\bar{I}_k = \sqrt{\bar{I}_{xk}^2 + \bar{I}_{zk}^2}$ from the complete model; (b) impulses $\bar{I}_{zk}$ from the simplified model.

sprockets and the chain spans. As the system's natural frequencies change, the responses of the sprockets and chain spans also change. Thus, the fluctuations in these impulses are caused by changes of the system's natural frequencies when α changes.

To examine further the difference between the impact intensities of the two models, in Figure 11(a) the averaged impulses ($\hat{I}_{avg}$) of the tight span over a range of sprocket rotational speeds are compared for a small J_1, J_2 and α combination. As discussed earlier, the impact intensities are frequency dependent. It can be seen that the impulses fluctuate around their mean values, and their mean values tend to increase with the sprocket rotational speeds. It is shown that the difference of the impulse magnitudes between two

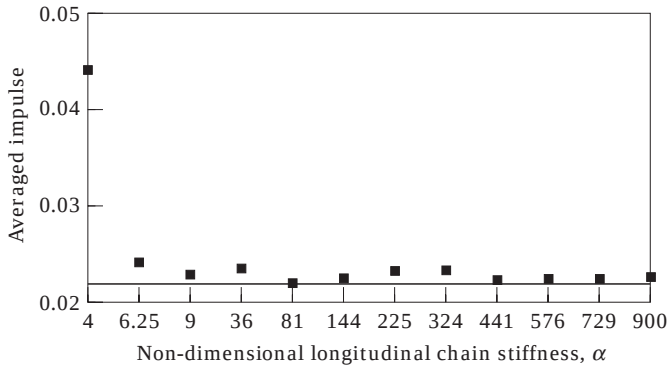

Figure 10. A comparison of the impulses between two models under various α, sprocket r.p.m. = 2500, $J_1 = 4$, $J_2 = 28$. ■, Complete model; ——, simplified model.

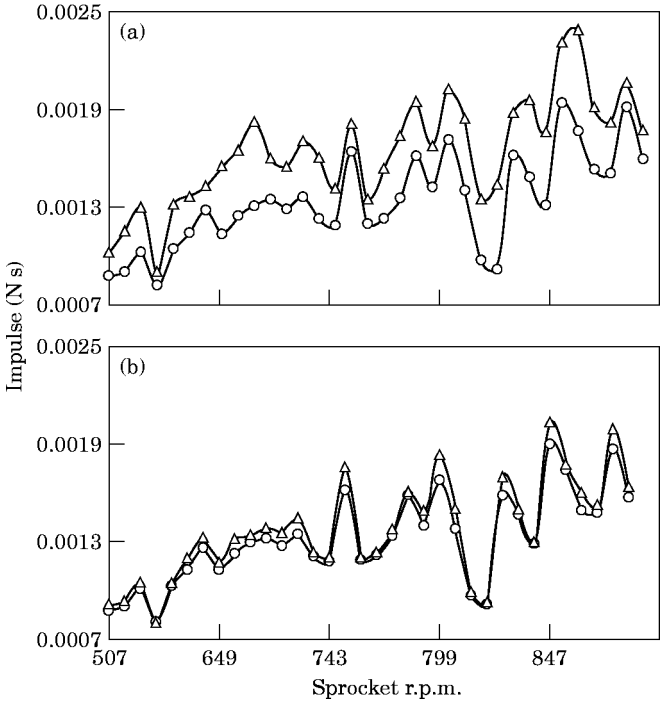

Figure 11. A comparison of the impulses between two models over a range of the sprocket rotational speeds. (a) $J_1 = J_2 = 0{\cdot}01$ and $\alpha = 1$; (b) $J_1 = 4$, $J_2 = 28$ and $\alpha = 975$. –○–, Simplified model; –△–, completed model.

models is significant through the computed speed range. This again illustrates that the coupling effects of the chain spans and sprockets on the impulses can be important when the sprocket inertia and chain longitudinal stiffness are small.

On the other hand, when J_1, J_2 and α are large, the chain longitudinal motion and sprocket effects on the impulses are reduced. In Figure 11(b) the averaged impulses ($\hat{I}_{avg}$) of the tight span of the two models over a range of the sprocket rotational speeds are compared for a large J_1, J_2 and α combination. It is shown that the difference of the impact intensities between the two models is small. This illustrates that the simplified model will be sufficient to predict impulses for a two-sprocket chain drive system for large J_1, J_2 and α conditions.

5. EXPERIMENTAL STUDIES

5.1. EXPERIMENTAL SET-UP

Experimental studies of the chain/sprocket meshing noise are performed to verify the analytical findings discussed above. In practice, the physical quantity of impulse is difficult to measure experimentally. However, the noise created by this impulsive force can be experimentally detected with the proper instrumentation, as shown in Figures 12 and 13. A direct relationship between the chain/sprocket meshing impulsive loads and the near field sound pressure levels has been illustrated in reference [17].

The test stand consists of a two sprocket configuration with a flywheel and a brake mounted on the driving and driven shafts, respectively. A 5 HP DC motor with an analog controller is used to drive the flywheel shaft via a belt drive set-up. The chain's static tension and sprocket center-to-center distance are varied by a unislide table. The static

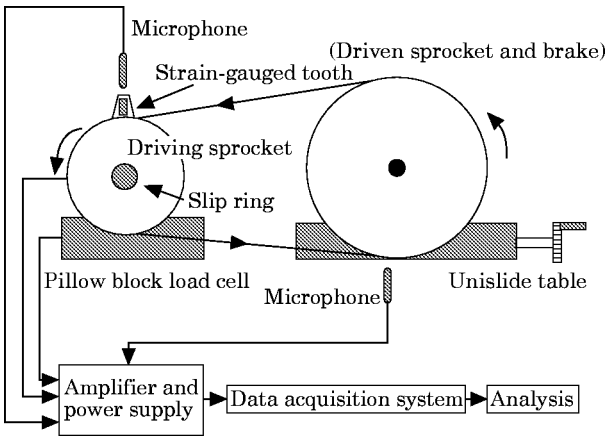

Figure 12. The experimental set-up.

tension and the dynamic load of the driving shaft are measured by an instrumented pillow block. The dynamic tensions of the chain spans are indirectly measured by a strain-gaged sprocket. A slip ring is installed to measure the rotational information of the driving shaft. Acoustical measurements are performed using two 1/2 inch microphones amplified by microphone amplifiers. The microphones are placed 1/2 inch away from the chain/sprocket engagement points. All measurements are performed inside a semi-anechoic room. A total

Figure 13. The chain testing hardware. 1, Frame; 2, hydraulic table; 3, hysteresis brake with coupler; 4, unislide table; 5, Compaq 386/20e with DAS-20; 6, HP analyzer; 7, electronic filters; 8, microphone amplifier; 9, microphone power supply; 10, oscilloscope; 11, current source; 12, power supply; 13, TSU tension readout; 14, strain gauge amplifier.

of 64 ensembles are averaged from the time signals to estimate the spectrum via a signal analyzer. A more detailed discussion on the experimental set-up is presented in reference [18].

5.2. EXPERIMENTAL RESULTS

In Figures 14(a) and (b) the meshing sound pressure levels measured experimentally (using the near-field microphone at the driving sprocket) are compared with impulses (tight span) computed from the analytical model. The operating parameters used in this investigation are listed in Table 1. Because the impulse and the sound pressure are different physical quantities, we will focus on examining the qualitative trend of the results. Comparing Figures 14(a) and (b), we see many similarities. It is shown that both the meshing sound pressure and the computed impulse are frequency dependent. Their amplitudes fluctuate and their mean values tend to increase with the sprocket speed. Some peak and valley locations (local maximum and minimum) of the impact noise amplitudes (Figure 14(a)) can be clearly captured in Figure 14(b). In other words, the meshing and resonant frequency effects predicted in the analytical models are clearly observed in the experimental results. It is also shown in Figure 14(b) that without considering the chain vibration and travelling speed, a classical quasi-static model cannot predict the impact intensity fluctuation, and significant errors could be induced. This confirms the merit of the new dynamic model over the classical approach.

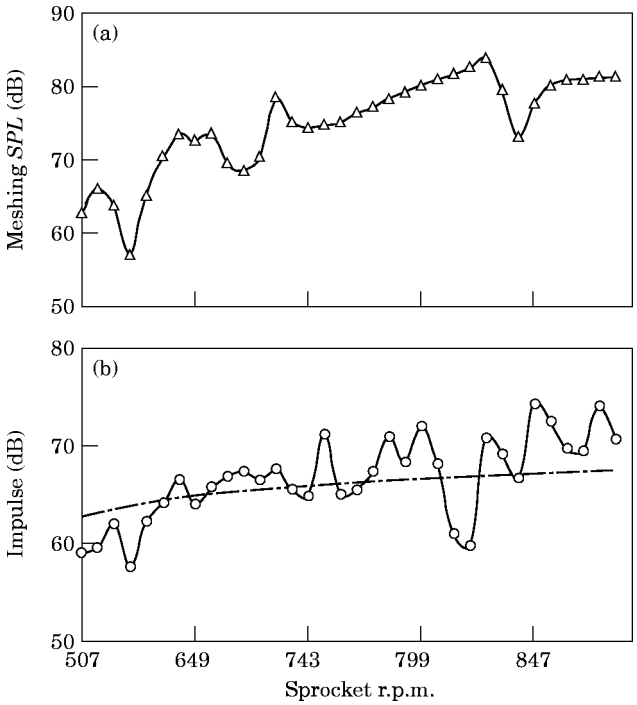

Figure 14. A comparison of the experimental meshing sound pressure levels and the analytically predicted impulses on the tight side of the chain span over a range of the sprocket rotational speeds. (a) Experimental meshing sound pressure levels; –△–, Experimental data. (b) Analytically predicted impulses: –○–, dynamic model; – · – · –, quasi-static model.

6. SUMMARY AND CONCLUSIONS

(1) A comprehensive model of a chain drive system is developed. The model integrates the sprocket and chain span motions with the local chain/sprocket meshing impacts. This model can describe the meshing dynamics when the chain/sprocket coupling effect is important.

(2) The relationship between the meshing frequency and the chain resonant frequency is important in determining the impact intensity. Meshing frequencies that will cause maximum and minimum impulses are predicted. It is concluded that the meshing impact magnitudes are highly frequency dependent.

(3) The effects of sprocket inertia and chain longitudinal stiffness on impact intensities have been investigated. It is found that the difference is significant between the impulses computed from the simplified model and those from the complete model when the chain longitudinal stiffness and sprocket inertia are small.

(4) The analytically computed impulses have been compared to the meshing sound pressure levels measured experimentally. The results verify the prediction that the meshing impulses and noise are frequency dependent, and confirm the merit of the dynamic model versus the classical quasi-static approach.

ACKNOWLEDGMENT

This research is supported by General Motors Corporation.

REFERENCES

1. D. N. Davis, P. J. Owen and G. Riley 1978 *Proceedings of Mechanisms I Mech E* **5**, 165–174. Roller chain camshaft drives.
2. R. C. Binder 1956 *Roller Chain Drive*, Englewood Cliffs, NJ: Prentice-Hall.
3. K. W. Wang and S. P. Liu 1991 *Shock and Vibration Digest* **23**(4), 8–13. On the noise and vibration of chain drive systems.
4. K. Uehara and T. Nakajima 1979 *Proceedings of the 5th World Congress on the Theory of Machines and Mechanisms*, *ASME*, 906–909. On the noise of roller chain driver.
5. W. A. Stone, M. W. Trethewey and K. W. Wang 1990 119*th Meeting of the ASA* **87**(1), s136. Experimental evaluation of chain noise.
6. M. S. Chew 1985 *Transactions of the American Society of Mechanical Engineers*, *Journal of Mechanisms*, *Transmission*, *and Automation in Design* **107**, 123–130. Inertia effect of a roller-chain on impact intensity.
7. J. N. Fawcett and S. W. Nicholl 1979 *Proceedings of the 5th World Congress on the Theory of Machines and Mechanisms*, *ASME* **2**, 1482–1485. A theoretical investigation of the vibrations of roller chain drives.
8. A. K. Kuznetsov and G. B. Stolbin 1958 *Trudy Mosstankina* **1**. Impact loading in chain drives.
9. G. K. Ryabov 1958 *Russian Engineering Journal* **48**(8), 17–19. Inertia effects of impact loading in chain drives.
10. K. W. Wang, S. P. Liu, S. I. Hayek and F. H. K. Chen 1992 *Transactions of the American Society of Mechanical Engineers*, *Journal of Vibration and Acoustics* **114**(3), 397–403. On the impact intensity of axially moving vibrating roller chains.
11. J. N. Fawcett and S. W. Nichol 1980 *Proceedings of Mechanisms I Mech E* **194**, 97–101. Vibration of a roller chain drive operating at constant speed and load.
12. S. W. Nichol and J. N. Fawcett 1977 *Proceedings of Mechanisms I Mech E* **191**, 363–370. Reduction of noise and vibration in roller chain drives.
13. S. R. Turnbull, S. W. Nichol and J. N. Fawcett 1977 *Design Engineering Technical Conference ASME* **77-Det-168**, 2–6. An experimental investigation of the dynamic behavior of a roller chain drive.
14. K. W. Wang 1992 *Transactions of the American Society of Mechanical Engineers*, *Journal of Vibration and Acoustics* **114**(1), 119–126. On the stability of chain drive systems under periodic sprocket oscillations.

15. J. Rismantab-Sany and A. A. Shabana 1990 *Journal of Vibration and Acoustics* **112**(1), 119–126. On the use of momentum balance in the impact analysis of constrained elastic systems.
16. A. Yigit, A. G. Ulsoy and R. A. Scott 1990 *Journal of Vibration and Acoustics* **112**(1), 65–70. Dynamics of a radial rotating beam with impact, part I: theoretical and computational model.
17. S. P. Liu 1994 *Thesis*, *Engineering Science and Mechanics*, *The Penn State University*. *Impact dynamics of chain drive systems*.
18. S. P. Liu, A. M. Dent, J. W. Thornton, M. W. Trethewey, K. W. Wang, S. I. Hayek and F. H. K. Chen 1995 *Proceedings of the* 1995 *Noise and Vibration Conference SAE* **P-291**(1), 33–42. Experimental evaluation of automotive timing chain drive impact noise.

APPENDIX A: EQUATIONS OF MOTION AND BOUNDARY CONDITIONS

The total kinetic energy, T, due to the chain span motions and sprocket motions is

$$T = \tfrac{1}{2}\int_0^L m\left[\left(s + \frac{\mathrm{d}\hat{u}}{\mathrm{d}t}\right)^2 + \left(\frac{\mathrm{d}\hat{w}}{\mathrm{d}t}\right)^2\right]\mathrm{d}x + \tfrac{1}{2}\int_0^L m\left[\left(-s + \frac{\mathrm{d}\hat{u}}{\mathrm{d}t}\right)^2 + \left(\frac{\mathrm{d}\hat{w}}{\mathrm{d}t}\right)^2\right]\mathrm{d}x$$

$$+ \tfrac{1}{2}\hat{J}_1\left(\frac{\mathrm{d}\theta_1}{\mathrm{d}t} + \frac{s}{r_1}\right)^2 + \tfrac{1}{2}\hat{J}_2\left(\frac{\mathrm{d}\theta_2}{\mathrm{d}t} + \frac{s}{r_2}\right)^2 \tag{A.1}$$

Here, $\mathrm{d}(\,)/\mathrm{d}t$ denotes a total derivative of time. The expression for the total potential energy is

$$U = U_1 + U_2 = \tfrac{1}{2}\int_0^L EA\left(\hat{u}' + \frac{\hat{w}'^2}{2} + \frac{R}{EA}\right)^2 \mathrm{d}x$$

$$+ \tfrac{1}{2}\int_0^L EA\left(\hat{\bar{u}}' + \frac{\hat{\bar{w}}'^2}{2} + \frac{\bar{R}}{EA}\right)^2 \mathrm{d}x, \tag{A.2}$$

where U_1 and U_2 denote the strain energies of chain spans.

The virtual work consists of the conservative and the non-conservative work:

$$\delta W_{total} = \delta W_c + \delta W_{nc}$$

$$= -\int_0^L (\hat{\bar{d}}_x\dot{\hat{\bar{u}}}\cdot\delta\hat{\bar{u}} + \hat{\bar{d}}_z\dot{\hat{\bar{w}}}\cdot\delta\hat{\bar{w}})\,\mathrm{d}x - \int_0^L (\hat{d}_x\dot{\hat{u}}\cdot\delta\hat{u} + \hat{d}_z\dot{\hat{w}}\cdot\delta\hat{w})\,\mathrm{d}x$$

$$- \hat{d}_1\left(\frac{\mathrm{d}\theta_1}{\mathrm{d}t} + \frac{s}{r_1}\right)\cdot\delta\theta_1 - \hat{d}_2\left(\frac{\mathrm{d}\theta_2}{\mathrm{d}t} + \frac{s}{r_2}\right)\cdot\delta\theta_2 + \hat{T}_1\cdot\delta\theta_1 + \hat{T}_2\cdot\delta\theta_2. \tag{A.3}$$

Using Hamilton's principle, one has

$$\delta H = \int_{t_1}^{t_2} (\delta T - \delta U + \delta W)\,\mathrm{d}t = 0. \tag{A.4}$$

With the non-dimensional parameters and variables listed in Appendix C, the equations of motion for $0 < \xi < 1$, and $\tau \geqslant 0$ are

$$\ddot{\bar{u}} + \bar{d}_x\dot{\bar{u}} - 2v\dot{\bar{u}}' - \Phi\bar{u}'' - \alpha\bar{w}'\bar{w}'' = 0, \tag{A.5}$$

$$\ddot{u} + d_x\dot{u} + 2v\dot{u}' - \Phi u'' - \alpha w'w'' = 0, \tag{A.6}$$

$$\ddot{\bar{w}} + \bar{d}_z\dot{\bar{w}} - 2v\dot{\bar{w}}' - \bar{\Psi}\bar{w}'' - \alpha(\bar{w}'\bar{u}'' + \bar{w}''\bar{u}') - \tfrac{3}{2}\alpha\bar{w}'^2\bar{w}'' = 0, \tag{A.7}$$

$$\ddot{w} + d_z\dot{w} + 2v\dot{w}' - \Psi w'' - \alpha(w'u'' + w''u') - \tfrac{3}{2}\alpha w'^2 w'' = 0. \tag{A.8}$$

The boundary conditions are

$$-\alpha\left(\bar{u}_0' + \frac{\bar{w}_0'^2}{2}\right) - \frac{J_1}{4\rho_1^2}(\ddot{u}_0 - \ddot{\bar{u}}_0) - \frac{d_1}{4\rho_1^2}(\dot{u}_0 - \dot{\bar{u}}_0) = 0, \tag{A.9}$$

$$-\alpha\left(u_0' + \frac{w_0'^2}{2}\right) + \frac{J_1}{4\rho_1^2}(\ddot{u}_0 - \ddot{\bar{u}}_0) + \frac{d_1}{4\rho_1^2}(\dot{u}_0 - \dot{\bar{u}}_0) = 0, \tag{A.10}$$

$$-\alpha\left(\bar{u}_1' + \frac{\bar{w}_1'^2}{2}\right) - \frac{J_2}{4\rho_2^2}(\ddot{u}_1 - \ddot{\bar{u}}_1) - \frac{d_2}{4\rho_2^2}(\dot{u}_1 - \dot{\bar{u}}_1) = 0, \tag{A.11}$$

$$-\alpha\left(u_1' + \frac{w_1'^2}{2}\right) + \frac{J_2}{4\rho_2^2}(\ddot{u}_1 - \ddot{\bar{u}}_1) + \frac{d_2}{4\rho_2^2}(\dot{u}_1 - \dot{\bar{u}}_1) = 0, \tag{A.12}$$

$$w(0, \tau) = \bar{w}(0, \tau) = 0 \tag{A.13}$$

and

$$w(1, \tau) = \bar{w}(1, \tau) = 0, \tag{A.14}$$

where $u_0 = u(0, \tau)$ and $\bar{u}_1 = \bar{u}(1, \tau)$, etc.

Based on assumptions (7) and (8), we neglect the non-linear elasticity coupling and apply the chain/sprocket impulsive loads to the equations of motion (A.5)–(A.14). The linearized system equations of motion are listed in equations (1)–(4) and (6)–(11).

APPENDIX B: MATRIX EXPRESSIONS

The impulsive forces in equations (1)–(4) are given as

$$\bar{f}_x = \sum_{k=1}^{N} \bar{I}_{xk}[\mathrm{H}(\xi - \xi_1) - \mathrm{H}(\xi - \xi_2)]\,\delta(\tau - \tau_k), \tag{B.1}$$

$$f_x = \sum_{k=1}^{N} I_{xk}[\mathrm{H}(\xi - \xi_1') - \mathrm{H}(\xi - \xi_2')]\,\delta(\tau - \tau_k), \tag{B.2}$$

$$\bar{f}_z = \sum_{k=1}^{N} \bar{I}_{zk}[\mathrm{H}(\xi - \xi_1) - \mathrm{H}(\xi - \xi_2)]\,\delta(\tau - \tau_k), \tag{B.3}$$

$$f_z = \sum_{k=1}^{N} I_{zk}[\mathrm{H}(\xi - \xi_1') - \mathrm{H}(\xi - \xi_2')]\,\delta(\tau - \tau_k), \tag{B.4}$$

where $\bar{I}_{xk}$ and I_{xk} are the axial components of impulse intensities on tight and slack spans, respectively, while $\bar{I}_{zk}$ and I_{zk} denote the transverse components of impulse intensities. $\mathrm{H}(\xi - \xi_1)$, $\mathrm{H}(\xi - \xi_2)$, $\mathrm{H}(\xi - \xi_1')$ and $\mathrm{H}(\xi - \xi_2')$ are unit step functions, and δ is the Dirac delta function.

In equations (1)–(4) and (6)–(11), the weighted functions are selected to be the same as the trial functions. Carrying out Galerkin's procedure, we have: the inertial matrices

$$M_{\bar{u}} = \int_0^1 \bar{h}_n(\xi) \cdot \bar{h}_m(\xi)\,\mathrm{d}\xi + \frac{J_1}{4\rho_1^2}\,\bar{h}_n(0) \cdot \bar{h}_m(0) + \frac{J_2}{4\rho_2^2}\,\bar{h}_n(1) \cdot \bar{h}_m(1), \tag{B.5}$$

$$M_u = \int_0^1 h_n(\xi) \cdot h_m(\xi)\,\mathrm{d}\xi + \frac{J_1}{4\rho_1^2}\,h_n(0) \cdot h_m(0) + \frac{J_2}{4\rho_2^2}\,h_n(1) \cdot h_m(1), \tag{B.6}$$

$$M_{\bar{w}} = \int_0^1 \bar{b}_n(\xi) \cdot \bar{b}_m(\xi)\,\mathrm{d}\xi = M_w; \tag{B.7}$$

the gyroscopic matrices

$$G_{\bar{u}} = -2v \int_0^1 \bar{h}_n'(\xi) \cdot \bar{h}_m(\xi)\,\mathrm{d}\xi, \qquad G_u = 2v \int_0^1 h_n'(\xi) \cdot h_m(\xi)\,\mathrm{d}\xi, \tag{B.8, B.9}$$

$$G_{\bar{w}} = -2v \int_0^1 \bar{b}_n'(\xi) \cdot \bar{b}_m(\xi)\,\mathrm{d}\xi = -G_w; \tag{B.10}$$

the damping matrices

$$D_{\bar{u}} = \bar{d}_x \int_0^1 \bar{h}_n(\xi) \cdot \bar{h}_m(\xi)\,\mathrm{d}\xi + \frac{d_1}{4}\,\bar{h}_n(0) \cdot \bar{h}_m(0) + \frac{d_2}{4}\,\bar{h}_n(1) \cdot \bar{h}_m(1),$$

$$D_u = d_x \int_0^1 h_n(\xi) \cdot h_m(\xi)\,\mathrm{d}\xi + \frac{d_1}{4}\,h_n(0) \cdot h_m(0) + \frac{d_2}{4}\,h_n(1) \cdot h_m(1),$$

$$D_{\bar{w}} = \bar{d}_z \int_0^1 \bar{b}_n(\xi) \cdot \bar{b}_m(\xi)\,\mathrm{d}\xi, \qquad D_w = d_z \int_0^1 b_n(\xi) \cdot b_m(\xi)\,\mathrm{d}\xi, \tag{B.13, B.14}$$

the stiffness matrices

$$K_{\bar{u}} = \Phi \int_0^1 \bar{h}_n''(\xi) \cdot \bar{h}_m(\xi)\,\mathrm{d}\xi - \alpha\bar{h}_n'(0) \cdot \bar{h}_m(0) + \alpha\bar{h}_n'(1) \cdot \bar{h}_m(1), \tag{B.15}$$

$$K_u = \Phi \int_0^1 h_n''(\xi) \cdot h_m(\xi)\,\mathrm{d}\xi - \alpha h_n'(0) \cdot h_m(0) + \alpha h_n'(1) \cdot h_m(1), \tag{B.16}$$

$$K_{\bar{w}} = \bar{\Psi} \int_0^1 \bar{b}_n''(\xi) \cdot \bar{b}_m(\xi)\, \mathrm{d}\xi, \qquad K_w = \Psi \int_0^1 b_n''(\xi) \cdot b_m(\xi)\, \mathrm{d}\xi; \qquad \text{(B.17, B.18)}$$

and the space vectors

$$Y_{\bar{u}} = -\int_0^1 \bar{h}_n(\xi)[\mathrm{H}(\xi - \xi_1) - \mathrm{H}(\xi - \xi_2)]\, \mathrm{d}\xi, \quad Y_u = \int_0^1 h_n(\xi)[\mathrm{H}(\xi - \xi_1') - \mathrm{H}(\xi - \xi_2')]\, \mathrm{d}\xi,$$

(B.19, B.20)

$$Y_{\bar{w}} = \int_0^1 \bar{b}_n(\xi)[\mathrm{H}(\xi - \xi_1) - \mathrm{H}(\xi - \xi_2)]\, \mathrm{d}\xi, \quad Y_w = -\int_0^1 b_n(\xi)[\mathrm{H}(\xi - \xi_1') - \mathrm{H}(\xi - \xi_2')]\, \mathrm{d}\xi,$$

(B.21, B.22)

APPENDIX C: NON-DIMENSIONAL PARAMETERS

$$d_x = \hat{d}_x L/mc, \qquad \bar{d}_x = \hat{\bar{d}}_x L/mc, \qquad d_z = \hat{d}_z L/mc, \qquad \bar{d}_z = \hat{\bar{d}}_z L/mc,$$

$$d_1 = \hat{d}_1/(mcL^2), \qquad d_2 = \hat{d}_2/(mcL^2), \qquad J_1 = \hat{J}_1/(mL^3), \qquad J_2 = \hat{J}_2/(mL^3),$$

$$u(\xi, \tau) = \hat{u}/L, \qquad \bar{u}(\xi, \tau) = \hat{\bar{u}}/L, \qquad V_{su} = V_{st} \cos \phi_2/\sqrt{R/m},$$

$$V_{s\bar{u}} = V_{st} \cos \phi_1/\sqrt{R/m}, \qquad V_{sw} = V_{st} \sin \phi_2/\sqrt{R/m}, \qquad V_{s\bar{w}} = V_{st} \sin \phi_1/\sqrt{R/m},$$

$$v = s/\sqrt{R/m}, \qquad w(\xi, \tau) = \hat{w}/L, \qquad \bar{w}(\xi, \tau) = \hat{\bar{w}}/L,$$

$$\alpha = EA/R, \qquad \Phi = \alpha - v^2, \qquad \Psi = 1 - v^2, \qquad \bar{\Psi} = \Psi + \hat{d}_1 s/(Rr_1^2),$$

$$\rho_1 = r_1/L, \qquad \rho_2 = r_2/L, \qquad \tau = t\sqrt{R/m}/L,$$

$$\xi = x/L, \qquad \xi_0 = x_0/L, \qquad \xi_0' = 1 - \xi_0,$$

$$\xi_1 = 0{\cdot}75\xi_0, \qquad \xi_2 = 1{\cdot}25\xi_0, \qquad \xi_1' = 1 - 0{\cdot}75\xi_0, \qquad \xi_2' = 1 - 1{\cdot}25\xi_0.$$

APPENDIX D: NOMENCLATURE

c	chain wave speed
$\hat{d}_x, \hat{\bar{d}}_x$	longitudinal damping coefficients of the slack and tight spans
$\hat{d}_z, \hat{\bar{d}}_z$	transverse damping coefficients of the slack and tight spans
$\hat{d}_1, \hat{d}_2$	rotational damping coefficients of the driving and driven sprockets
EA	longitudinal elastic constant
$f, \bar{f}$	resultant forcing functions of the slack and tight spans
$f_x, \bar{f}_x$	longitudinal forcing functions of the slack and tight spans
$f_z, \bar{f}_z$	transverse forcing functions of the slack and tight spans
$I_k, \bar{I}_k$	resultant impact intensities of the slack and tight spans
$I_{xk}, \bar{I}_{xk}$	longitudinal impact intensities of the slack and tight spans
$I_{zk}, \bar{I}_{zk}$	transverse impact intensities of the slack and tight spans
$\hat{I}_{avg}$	averaged impact intensity
$\hat{J}_1, \hat{J}_2$	rotational inertias of the driving and driven sprockets
L	chain span length
$\hat{M}_1, \hat{M}_2$	masses of the driving and driven sprockets

m	mass per length of the chain
R, $\bar{R}$	chain initial tensions (slack and tight spans)
r_1, r_2	radii of the driving and driven sprockets
s	chain nominal axial speed
$\hat{T}_1$, $\hat{T}_2$	torques applied on driving and driven sprockets
$\hat{u}$, $\hat{\bar{u}}$	longitudinal displacements of the slack and tight spans
V_{st}	tangential speed of the sprocket tooth at the sprocket pitch circle
$\hat{w}$, $\hat{\bar{w}}$	transverse displacements of the slack and tight spans
x	longitudinal axis of the chain span
x_0	chain link pitch
ϕ_1, ϕ_2	half-pitch angles of driving and driven sprockets
θ_1, θ_2	rotational displacements of the driving and driven sprockets